Knotted trajectories of neutral and charged particles in Gaussian light beams

Tomasz Radożycki*

Faculty of Mathematics and Natural Sciences, College of Sciences, Institute of Physical Sciences, Cardinal Stefan Wyszyński University, Wóycickiego 1/3, 01-938 Warsaw, Poland

(Received 14 May 2020; accepted 16 November 2020; published 1 December 2020)

Making use of the equivalence between the paraxial wave equation and two-dimensional Schrödinger equation, Gaussian beams of monochromatic light, possessing knotted nodal structures, are obtained in an analytical way. These beams belong to the wide class of paraxial beams called the hypergeometric-Gaussian beams [E. Karimi, G. Zito, B. Piccirillo, L. Marrucci, and E. Santamato, Opt. Lett. **32**, 3053 (2007)]. Four topologies are dealt with: the unknot, the Hopf link, the $(3, 3)$-torus knot, and the trefoil. It is shown in a numerical way that neutral polarizable particles placed in such light fields, upon precise tuning of the initial conditions, can be forced to follow identical knotted trajectories. A similar outcome is also valid for charged particles that are subject to a ponderomotive potential. This effect can serve to precisely steer particles along chosen complicated pathways exhibiting nontrivial topological character, guide them around obstacles, and, depending on the knot size, seems to provide help in engineering more complex nanoparticles.

DOI: 10.1103/PhysRevA.102.063101

I. INTRODUCTION

In recent years, it has been proved possible to investigate and generate beams of light with some complex structure far from the academic concept of plane waves. Theoretical and experimental studies of "structured" light and "non-diffracting" or "accelerating" beams have been developed [1–8], opening a variety of possible applications, in particular for trapping and guiding particles, atoms, molecules, or even micrometer-sized objects. Among beams that have gained special interest, one can enumerate Laguerre-Gaussian [9–11], Bessel [11–16], Airy [4,17,18], and Mathieu [19,20] beams.

A relatively new idea is that of the "knotted" light, although topological concepts have long been present in physics [21–23]. The term "knot" refers to the characteristics of electric or magnetic field lines [24–29], which can get entangled, or of the nodal lines of the wave intensity, or of optical vortex lines [30–35]. It has become possible from the experimental point of view to generate such knotted beams [36–39], thus creating the opportunity for practical use.

It is well known that the nonhomogeneities of the electric field can provide gradient forces for trapping atoms due to the Stark effect [40] or, equivalently, due to the polarizability of atoms. This phenomenon provides the basis for a trap called the optical tweezer [41,42]. Assuming the atomic dipole moment to be proportional to the external electric field, the atomic polarizability α (in general depending on the driving frequency) can be introduced as

$$\boldsymbol{d} = \alpha \boldsymbol{E}. \tag{1}$$

This leads to the equation of motion of an atom in the form

$$m\ddot{\boldsymbol{r}} = (\boldsymbol{d} \cdot \nabla)\boldsymbol{E} = \tfrac{1}{2}\,\alpha \nabla (E^2). \tag{2}$$

From the theory of the Stark effect in atoms it is known that for a blue-detuned beam the polarizability α becomes negative [43]. This causes particles to be dragged into an area with a lower value of E^2. A natural question arises whether the knotted nodal lines spoken of above can serve as traps for this kind of particle [38]. One might expect that the considered knots constituting regions of weaker field should attract atoms with $\alpha < 0$. A similar effect should be observed for charged particles, (e.g., electrons), moving in the ponderomotive potential, where the coefficient α is negative as well [15]. So, one can ask an important question: Can all these particles be forced to move along previously chosen and designed knotted paths? To our knowledge, this interesting issue has not been studied so far. Some simpler trajectories such as rings or helices have already been shown to be actually realized, for instance in Bessel beams [16]. It seems worthy of some attention to verify whether the knotted structure can be transferred from the field to particles. This might open a variety of applications including the guidance of particles around special kinds of obstacles, the engineering of complex nanoparticles (if knots are made small enough), or the generation of knotted nanocircuits (e.g., for electrons that are subject to ponderomotive force).

The manipulation of particles has become an extremely topical and important issue in recent years due to the significant applications in physics, chemistry, biology, and medicine (see for instance [44–50]). The knotted trajectories would constitute a new and potentially widely applicable family and we hope that current work adds a tiny contribution in this regard. Motion of charged particles in the knotted electromagnetic field (but in the sense of the field-lines' knots) was dealt with in [51].

*t.radozycki@uksw.edu.pl

As mentioned above, knots understood as nodal lines create some kind of potential valleys for particles in question. Their guidance along these lines is, however, a highly nontrivial issue, since the tightly knotted lines disturb the structure of these valleys and make them substantially shallower, which can knock particles out of their designed trajectories. In this work it is shown that the particles can still follow knotted paths if the initial conditions are carefully tuned.

Let us express the complex electric field of a monochromatic wave through an envelope $\Psi(\boldsymbol{r})$:

$$\boldsymbol{E}(\boldsymbol{r},t)=\boldsymbol{E}_0 e^{i(kz-\omega t)}\Psi(\boldsymbol{r}), \tag{3}$$

where $\boldsymbol{E}_0$ is a constant vector. Below it will be convenient to make use of the dimensionless coordinates

$$\xi_x=kx,\quad \xi_y=ky,\quad \xi=\sqrt{\xi_x^2+\xi_y^2},\quad \zeta=kz, \tag{4}$$

where $k=\omega/c$. In our approach, the third component plays a special role, so we prefer to denote it with the symbol ζ instead of ξ_z. These variables turned out to be convenient in our previous papers dealing with trapping of particles by light beams. However, for the convenience of the reader some of the knotted beams finally obtained in the subsequent sections will be given more traditional form as well.

In what follows, the bold mathematical symbols refer to two-dimensional vectors, for instance $\boldsymbol{\xi}=[\xi_x,\xi_y]$. Similarly $\boldsymbol{r}=[x,y]$.

After having averaged the potential on the right-hand side of (2) over fast optical oscillations, one gets the smoothed equations of motion in the form

$$\ddot{\boldsymbol{\xi}}=-\beta\boldsymbol{\partial}_{\xi}|\Psi|^2,\quad \ddot{\zeta}=-\beta\partial_{\zeta}|\Psi|^2, \tag{5}$$

where $\beta=|\alpha||E_0|^2/4mc^2$ and ∂_x denotes $\partial/\partial x$. For laser intensities in the range of 10^7–10^8 W/cm^2 one can achieve a depth of the appropriate potential valley of the order of a couple of meV, depending also on the atomic polarizability. The trap then still remains perturbative in the sense that it does not significantly interfere with the internal structure of atomic energy levels. The figures below are of illustrative character and are performed for the value of β equal to 10^{-2} for reasons of clear visualization. For smaller values of β the trap is still operative, but the particles require very precise preparation of the initial states, particularly with respect to the transverse velocities. For electrons subject to ponderomotive force the value of β may be increased, which corresponds to proportionally stronger laser fields.

In the following sections we first describe how to theoretically construct Gaussian beams with a given knotted topology and then, using (5), the results of the numerical integration, demonstrating particle trajectories for four special knots [the unknot, the Hopf link, the $(3,3)$-torus knot, and the trefoil], are presented.

II. GAUSSIAN BEAMS WITH NODAL KNOTS

One can treat a knot as a closed curve in $\mathbb{R}^3$, i.e., a curve that constitutes a homeomorphic image of S^1. It then forms a loop. This curve may be a nodal line of a certain complex-valued function of the spatial variables x,y,z (in our case ξ_x,ξ_y,ζ). Of course, a knot can also be composed of several disjoint loops, that are tangled up forming a link (e.g., the Hopf link, the Borromean rings, and so on).

The construction leading to the required specific knots or links can be found elsewhere [32,52–54]. The details remain beyond the scope of this work and we will limit ourselves to mentioning the main steps only. First, one constructs a polynomial $q(u,v)$ of two complex variables u and v which satisfy the condition for the three-dimensional sphere: $|u|^2+|v|^2=1$. The examples of such polynomials are given in the following section. All points where $q(u,v)=0$ represent an algebraic knot.

Since we are concerned about knots in $\mathbb{R}^3$ rather than on S^3, the next step is to use the stereographic projection by means of the relations

$$u(\boldsymbol{\xi},\zeta)=\frac{\boldsymbol{\xi}^2+\zeta^2-1+2i\zeta}{\boldsymbol{\xi}^2+\zeta^2+1}, \tag{6a}$$

$$v(\boldsymbol{\xi},\zeta)=\frac{2(\xi_x+i\xi_y)}{\boldsymbol{\xi}^2+\zeta^2+1}, \tag{6b}$$

and to require $q(u(\boldsymbol{\xi},\zeta),v(\boldsymbol{\xi},\zeta))=0$. In that way the knot curve becomes an intersection of two surfaces in three-dimensional space: $\mathrm{Re}\,q(u(\boldsymbol{\xi},\zeta),v(\boldsymbol{\xi},\zeta))=0$ and $\mathrm{Im}\,q(u(\boldsymbol{\xi},\zeta),v(\boldsymbol{\xi},\zeta))=0$. Since $q(u,v)$ is a polynomial, $q(u(\boldsymbol{\xi},\zeta),v(\boldsymbol{\xi},\zeta))$ can again be treated as a polynomial (called the Milnor polynomial [55]), upon removing the common denominator stemming from (6). For the appropriate Milnor polynomial the symbol $q_M(\boldsymbol{\xi},\zeta)$ is reserved below.

The knot lines obtained that way cannot, however, constitute nodal lines of light waves since, in general, the wave equation would not be satisfied. We are rather interested in special superpositions of Gaussian beams which, on one hand, satisfy the paraxial equation

$$\triangle\Psi(\boldsymbol{\xi},\zeta)+2i\partial_{\zeta}\Psi(\boldsymbol{\xi},\zeta)=0, \tag{7}$$

with $\triangle$ denoting the two-dimensional Laplace operator in variables $\boldsymbol{\xi}$, and, on the other hand, exhibit knotted nodal lines. In order to construct such waves the obvious equivalence of (7) to the two-dimensional Schrödinger equation for a free particle,

$$-\frac{\hbar^2}{2m}\triangle\Psi(\boldsymbol{r},t)=i\hbar\partial_t\Psi(\boldsymbol{r},t), \tag{8}$$

can be made use of. These two equations become identical upon the identifications

$$mc^2=\hbar\omega,\quad \boldsymbol{\xi}=k\boldsymbol{r},\quad \zeta=\omega t. \tag{9}$$

Therefore, instead of talking about waves satisfying the paraxial equation one can consider the time evolution of a free-particle's wave function in two dimensions. The time-dependent (or ζ-dependent) wave function which coincides with the relevant Milnor polynomial (eventually with a Gaussian factor) at $t=0$ (i.e., on the surface $\zeta=0$) and evolves according to Eq. (8) will inherit from that polynomial the topological structure of the nodal lines.

The evolution of a free particle in quantum mechanics is, obviously, well known and is determined by the Schrödinger

propagator which, in two spatial dimensions, has the form

$$K(\boldsymbol{r},t;\boldsymbol{r}',t') = \frac{-im}{2\pi\hbar(t-t')}\exp\left[i\frac{m(\boldsymbol{r}-\boldsymbol{r}')^2}{2\hbar(t-t')}\right]. \tag{10}$$

It follows then that the function $\Psi(\boldsymbol{\xi},\zeta)$,

$$\Psi(\boldsymbol{\xi},\zeta) = \int d^2\xi' K(\boldsymbol{\xi},\zeta;\boldsymbol{\xi}',0)e^{-\kappa\xi'^2}q_M(\boldsymbol{\xi}',0), \tag{11}$$

where $\kappa > 0$ and

$$K(\boldsymbol{\xi},\zeta;\boldsymbol{\xi}',\zeta') = \frac{-i}{2\pi(\zeta-\zeta')}\exp\left[i\frac{(\boldsymbol{\xi}-\boldsymbol{\xi}')^2}{2(\zeta-\zeta')}\right], \tag{12}$$

fulfills the paraxial equation (7), while maintaining the desired knotted structure of the nodal lines and the Gaussian character (at least for a mild Gaussian). Apparently $K(\boldsymbol{\xi},\zeta;\boldsymbol{\xi}',\zeta')$ does not satisfy the paraxial condition due to the divergence as $\zeta \to \zeta'$, but one should remember that this behavior is smoothed out thanks to the integration in (11).

III. KNOTTED TRAJECTORIES OF PARTICLES

In this section four specific examples of such knotted lines are dealt with: the unknot (i.e., the ring), the Hopf link, the (3, 3)-torus knot, and the trefoil. The first three examples are generated from the polynomial $q(u,v)$, which can be written in the general form

$$q(u,v) = \prod_{k=0}^{n-1}\left(u - \varepsilon_n^{(k)}v\right), \tag{13}$$

where $\varepsilon_n^{(k)}$, $k = 0, 1, 2, \ldots, n-1$, denote the subsequent nth roots of unity.

A. The unknot

The polynomial $q(u,v)$ to generate a ring is obtained by inserting $n = 1$ into (13), which leads to

$$q(u,v) = u - v. \tag{14}$$

Substituting u and v in the form of (6), the Milnor polynomial at $\zeta = 0$ is obtained as

$$q_M(\boldsymbol{\xi},0) = -1 + \xi_x^2 + \xi_y^2 - 2(\xi_x + i\xi_y). \tag{15}$$

In order to keep the possibility of modifying the spatial size of the knot, here, and in the following examples, an additional scaling factor γ will be introduced wherever the powers ξ_x and ξ_y occur. This procedure does not change the topology of the knot, but offers the possibility to adjust its size to the dimensions achievable in an experiment and to those needed in for a particular application. There are, therefore, experimental limits for the admissible values of γ. The value adopted in this work (i.e., $\gamma = 2\times10^{-2}$) fully satisfies these requirements. Consequently, instead of (15) we will use

$$q_M(\boldsymbol{\xi},0) = -1 + \gamma^2\left(\xi_x^2 + \xi_y^2\right) - 2\gamma(\xi_x + i\xi_y). \tag{16}$$

This leads to the paraxial envelope in the form

$$\Psi(\boldsymbol{\xi},\zeta) = \frac{-i}{2\pi\zeta}\int_0^\infty d\xi'\xi'\int_0^{2\pi}d\phi' e^{\frac{i}{2\zeta}[\xi^2+\xi'^2-2\xi\xi'\cos(\phi-\phi')]} \times e^{-\kappa\xi'^2}(-1+\gamma^2\xi'^2 - 2\gamma\xi' e^{i\phi'}), \tag{17}$$

where polar coordinates have been introduced. The subsequent integrals over ϕ' and ξ' can be easily calculated with the use of the formulas in the Appendix, with the following result:

$$\Psi(\boldsymbol{\xi},\zeta) = \frac{i}{\zeta}e^{\frac{i}{2\zeta}\xi^2}\int_0^\infty d\xi' e^{-(\kappa-\frac{i}{2\zeta})\xi'^2} \times[\xi'(1-\gamma^2\xi'^2)J_0(\xi\xi'/\zeta) - 2ie^{i\phi}\gamma\xi'^2 J_1(\xi\xi'/\zeta)], \tag{18}$$

with J_n denoting the Bessel functions, and then

$$\Psi(\boldsymbol{\xi},\zeta) = e^{-\frac{\kappa\xi^2}{c(\zeta)}}\left(\frac{-1}{c(\zeta)} + \frac{2i\gamma^2\zeta}{c(\zeta)^2} + \frac{\gamma^2\xi^2}{c(\zeta)^3} - \frac{2\gamma\xi}{c(\zeta)^2}e^{i\phi}\right), \tag{19}$$

where $c(\zeta) = 2i\kappa\zeta + 1$. As can be easily verified, the function $\Psi(\boldsymbol{\xi},\zeta)$ obtained above satisfies the paraxial equation (7). The role of the factors γ introduced in (16) merely reduces to fixing the relative intensities when superimposing various Gaussian beams in (19). This expression may be rewritten in more traditional but less convenient indications, if it is noticed that

$$c(\zeta) = 1 + i\frac{z}{z_R}, \tag{20a}$$

$$\kappa = \frac{1}{k^2w_0^2}, \tag{20b}$$

$$\frac{1}{c(\zeta)} = \frac{w_0}{w(z)}e^{-i\psi(z)}, \tag{20c}$$

where z_R is the Rayleigh length, w_0 denotes the beam waist, $w(z) = w_0\sqrt{1+(z/z_R)^2}$ is the beam radius, $R(z) = z[1+(z_R/z)^2]$ stands for the wavefront curvature and $\psi(z) = \arctan(z/z_R)$ is the Gouy phase. Expression (19) then takes the form ($\boldsymbol{r}$ refers to the transverse coordinates only)

$$\Psi(\boldsymbol{r},z) = \frac{w_0}{w(z)}\exp\left[-\frac{r^2}{w(z)^2} - i\frac{r^2k}{2R(z)} - i\psi(z)\right] \times\left(-1+\frac{2i\gamma kz}{1+iz/z_R} + \frac{\gamma^2k^2r^2}{(1+iz/z_R)^2} - \frac{2\gamma kre^{i\phi}}{1+iz/z_R}\right), \tag{21}$$

This beam belongs to the wide class of the so-called hypergeometric-Gaussian beams, theoretically described in [56] and experimentally created with the use of a computer-generated hologram and spatial light modulator. All beams representing more complicated knots obtained in the following subsections can be given the similar form.

Coming back to (19), one should consider two special limits. For $\kappa \to 0$ one has $c(\zeta) \to 1$, and the appropriate paraxial polynomial is recovered

$$q_p(\boldsymbol{\xi},\zeta) = -1 + 2i\gamma^2\zeta + \gamma^2\xi^2 - 2\gamma(\xi_x + i\xi_y). \tag{22}$$

It still constitutes the solution of the paraxial equation and possesses the same knotted structure, but cannot represent the true light wave due to its spatial divergence at infinity. In turn, letting $\zeta \to 0$ the function (16) tempered with the Gaussian is obtained. This is obvious from the very construction of the envelope Ψ, since the Schrödinger propagator satisfies

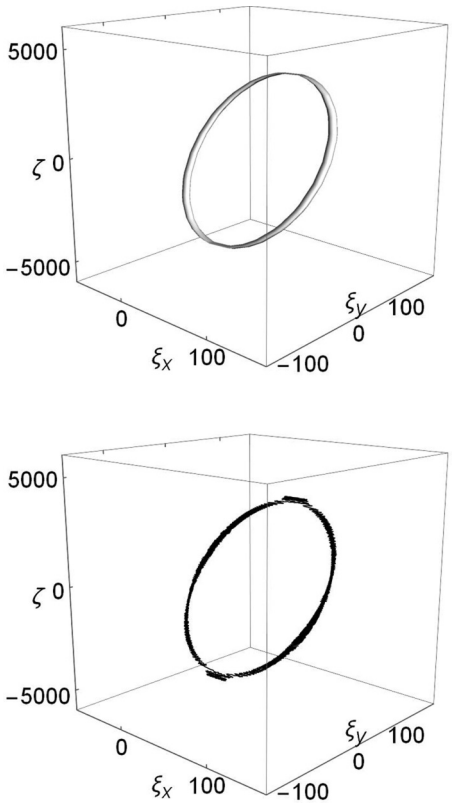

FIG. 1. The nodal line of the light wave representing the simplest "knot" (upper plot), and the trajectory of the injected particle (lower plot). The values of parameters are $\kappa = 10^{-8}$, $\beta = 10^{-2}$, $\gamma = 0.02$. The quantities on axes are dimensionless according to (4).

the condition

$$\lim_{t\to t'} K(\boldsymbol{r}, t; \boldsymbol{r}', t') = \delta^{(2)}(\boldsymbol{r} - \boldsymbol{r}'). \tag{23}$$

With this form of $\Psi(\boldsymbol{\xi}, \zeta)$ the equation of motion (5) of the particle can be numerically solved. The results for the value $\gamma = 2 \times 10^{-2}$ are presented in Fig. 1. It is visible that the particle exactly follows the nodal line of the wave, thereby moving along the knotted trajectory. The obtained trajectory is limited to the size of order $10^2\lambda$–$5 \times 10^3\lambda$, which justifies the adoption of the paraxial approximation spoken of below. This applies to all trajectories obtained in this work.

In order to discuss the relevance of the paraxial approximation for the trajectory of Fig. 1 (and for those of the subsequent figures as well), consider as an example the He-Ne laser with the wavelength of the emitted light of $\lambda = 632.8$ nm and the beam waist $w_0 = 1$ mm. The Rayleigh length for such a beam equals $z_R = \pi w_0^2/\lambda \approx 4.96$ m. The quantity κ is connected with the beam waist [see (20b)] and in these conditions $\kappa \approx 10^{-8}$. This small value is merely due to the units chosen (the length is measured in $\lambda/2\pi$). Since $\lambda/w_0 \approx 6.3 \times 10^{-4}$, then the radial extension of the trajectory is of order $10^2\lambda/2\pi \approx 10^{-2}w_0$. For the longitudinal extension, one has $5 \times 10^3\lambda/2\pi \approx 10^{-4}z_R$. These estimations justify the use of the paraxial approximation and equally, or even better, hold for all the trajectories obtained in this work and stay in agreement with the approximations used [57]. If necessary, the knotted structures and particle trajectories can be reduced to nanoscale sizes by increasing the value of γ (or enlarged by decreasing it). The results have been numerically tested up to $\gamma = 10$, which allows one to shrink the size of knots to the extreme value of 0.2λ. It turns out that the values of the parameters may be changed within wide limits, without significant modifications of the outcome (in the topological sense).

Apart from the motion along the nodal line of the electromagnetic wave, the particle performs an oscillatory motion perpendicular to it. The amplitude of these oscillations depends on the depth of the binding-potential valley, i.e., on the intensity of the wave, and on the initial tuning of the position and velocity.

B. The Hopf link

In order to obtain the Hopf link, one has to set $n = 2$ in (13), obtaining

$$q(u, v) = (u - v)(u + v). \tag{24}$$

The appropriate Milnor polynomial, found by substituting u and v according to (6) and reduced to the plane $\zeta = 0$, has now the form

$$q_M(\boldsymbol{\xi}, 0) = \left(1 - \xi_x^2 - \xi_y^2\right)^2 - 4(\xi_x + i\xi_y)^2. \tag{25}$$

Following the procedure outlined in the case of the unknot and introducing the scale parameter γ, one finds

$$\Psi(\boldsymbol{\xi}, \zeta) = \frac{-i}{2\pi\zeta} \int_0^\infty d\xi' \xi' \int_0^{2\pi} d\phi' e^{\frac{i}{2\zeta}[\xi^2 + \xi'^2 - 2\xi\xi'\cos(\phi - \phi')]} \times e^{-\kappa\xi'^2}[(1 - \gamma^2\xi'^2)^2 - 4\gamma^2\xi'^2 e^{2i\phi'}], \tag{26}$$

and consequently

$$\Psi(\boldsymbol{\xi}, \zeta) = \frac{-i}{\zeta} e^{\frac{i}{2\zeta}\xi^2} \int_0^\infty d\xi' e^{-(\kappa - \frac{i}{2\zeta})\xi'^2}[\xi'(1 - \gamma^2\xi'^2)^2 \times J_0(\xi\xi'/\zeta) + 4e^{2i\phi}\gamma^2\xi'^2 J_2(\xi\xi'/\zeta)], \tag{27}$$

where again the integrals collected in the Appendix have been used. This leads to the paraxial wave function

$$\Psi(\boldsymbol{\xi}, \zeta) = e^{-\frac{\kappa\xi^2}{c(\zeta)}}\left(\frac{1}{c(\zeta)} - \frac{4i\gamma^2\zeta}{c(\zeta)^2} - \frac{2\gamma^2\xi^2}{c(\zeta)^3} - \frac{8\gamma^4\zeta^2}{c(\zeta)^3} + \frac{8i\gamma^4\zeta\xi^2}{c(\zeta)^4} + \frac{\gamma^4\xi^4}{c(\zeta)^5} - \frac{4\gamma^2\xi^2}{c(\zeta)^3}e^{2i\phi}\right), \tag{28}$$

possessing nodal lines representing the Hopf link. Using the relations (20), the expression (28) can be easily given the form of a superposition of the Hypergeometric-Gaussian modes similar to (21):

$$\Psi(\boldsymbol{r}, z) = \frac{w_0}{w(z)} \exp\left[-\frac{r^2}{w(z)^2} - i\frac{r^2 k}{2R(z)} - i\psi(z)\right] \times \left(1 - \frac{4i\gamma^2 kz}{1 + iz/z_R} - \frac{2\gamma^2 k^2 r^2}{(1 + iz/z_R)^2} - \frac{8\gamma^4 k^2 z^2}{(1 + iz/z_R)^2} + \frac{8i\gamma^4 k^3 r^2 z}{(1 + iz/z_R)^3} + \frac{\gamma^4 k^4 r^4}{(1 + iz/z_R)^4} - \frac{4\gamma^2 k^2 r^2 e^{2i\phi}}{(1 + iz/z_R)^2}\right). \tag{29}$$

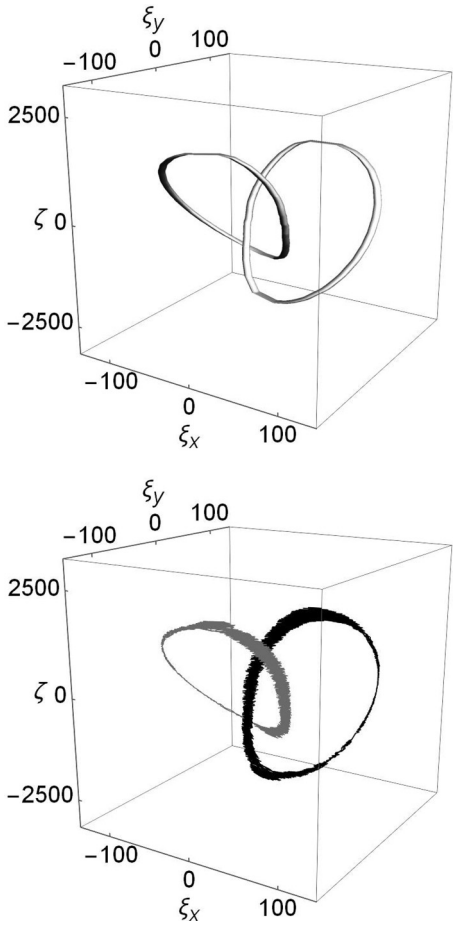

FIG. 2. The nodal line of the light wave representing the Hopf link (upper plot) and the trajectories of two injected particles (lower plot). The values of parameters are the same as in Fig. 1.

If $\kappa \to 0$, the paraxial polynomial is obtained as

$$q_p(\boldsymbol{\xi}, \zeta) = 1 - 4i\gamma^2\zeta - 2\gamma^2\left(\xi_x^2 + \xi_y^2\right) - 8\gamma^4\zeta^2 + 8i\gamma^4\zeta\left(\xi_x^2 + \xi_y^2\right) + \gamma^4\left(\xi_x^2 + \xi_y^2\right)^2 - 4\gamma^2(\xi_x + i\xi_y)^2. \tag{30}$$

The trajectories of two particles moving according to Eqs (5) with $\Psi(\boldsymbol{\xi}, \zeta)$ given by (28) are drawn in Fig. 2. As can be seen, each particle follows one of the two rings constituting the Hopfian.

Looking closely at the trajectories, one can again recognize the oscillatory motion in perpendicular directions. Upon precise examination, the amplitude of these oscillations turns out to increase in places where both rings are passing each other (the apparent broadening of the trajectories appears); this is due to the local flattening of the particle-binding potential. By this we mean the effect that as two potential minima approach each other the barrier between them gets lower. These are also places where a possible jump of the particle between the rings can eventually occur if the initial conditions are not sufficiently tuned. For more complex knots, this effect sets higher requirements regarding the preparation of the initial states of the particles. A more detailed discussion is given in the next section and at the end of Sec. III D.

C. The (3,3)-torus knot

The link known as the (3, 3)-torus knot is composed of three loops, and, therefore, one has to set $n = 3$ in (13), obtaining

$$q(u, v) = (u - v)(u - e^{2\pi i/3}v)(u - e^{4\pi i/3}v). \tag{31}$$

Consequently

$$q_M(\boldsymbol{\xi}, 0) = \left(-1 + \xi_x^2 + \xi_y^2\right)^3 - 8(\xi_x + i\xi_y)^3, \tag{32}$$

and, similarly as before,

$$\Psi(\boldsymbol{\xi}, \zeta) = \frac{-i}{2\pi\zeta}\int_0^\infty d\xi'\xi'\int_0^{2\pi} d\phi' e^{\frac{i}{2\zeta}[\xi^2 + \xi'^2 - 2\xi\xi'\cos(\phi - \phi')]} \times e^{-\kappa\xi'^2}[(-1 + \gamma^2\xi'^2)^3 - 8\gamma^3\xi'^3 e^{3i\phi'}]. \tag{33}$$

Using the integrals listed in the Appendix, we first come to

$$\Psi(\boldsymbol{\xi}, \zeta) = \frac{-i}{\zeta} e^{\frac{i}{2\zeta}\xi^2}\int_0^\infty d\xi' e^{-(\kappa - \frac{i}{2\zeta})\xi'^2}[\xi'(-1 + \gamma^2\xi'^2)^3 \times J_0(\xi\xi'/\zeta) - 8ie^{3i\phi}\gamma^3\xi'^3 J_3(\xi\xi'/\zeta)], \tag{34}$$

and finally get the paraxial envelope as

$$\Psi(\boldsymbol{\xi}, \zeta) = e^{-\frac{\kappa\xi^2}{c(\zeta)}}\left(\frac{-1}{c(\zeta)} + \frac{6i\gamma^2\zeta}{c(\zeta)^2} + \frac{3\gamma^2\xi^2}{c(\zeta)^3} + \frac{24\gamma^4\zeta^2}{c(\zeta)^3} - \frac{48i\gamma^6\zeta^3}{c(\zeta)^4} - \frac{24i\gamma^4\xi^2\zeta}{c(\zeta)^4} - \frac{72\gamma^6\xi^2\zeta^2}{c(\zeta)^5} - \frac{3\gamma^4\xi^4}{c(\zeta)^5} + \frac{18i\gamma^6\xi^4\zeta}{c(\zeta)^6} + \frac{\gamma^6\xi^6}{c(\zeta)^7} - \frac{8\gamma^3\xi^3}{c(\zeta)^4}e^{3i\phi}\right). \tag{35}$$

This envelope could again be represented as a combination of hypergeometric-Gaussian beams in an obvious way, but there is no need to write down the explicit formula here [and after formula (42)].

The corresponding paraxial polynomial has the form

$$q_p(\boldsymbol{\xi}, \zeta) = -1 + 6i\gamma^2\zeta + 3\gamma^2\left(\xi_x^2 + \xi_y^2\right) + 24\gamma^4\zeta^2 - 48i\gamma^6\zeta^3 - 24i\gamma^4\left(\xi_x^2 + \xi_y^2\right)\zeta - 72\gamma^6\left(\xi_x^2 + \xi_y^2\right)\zeta^2 - 3\gamma^4\left(\xi_x^2 + \xi_y^2\right)^2 + 18i\gamma^6\left(\xi_x^2 + \xi_y^2\right)^2\zeta + \gamma^6\left(\xi_x^2 + \xi_y^2\right)^3 - 8\gamma^3(\xi_x + i\xi_y)^3. \tag{36}$$

Now one can pass to the motion of atoms accurately injected into the electromagnetic field (35). The numerical calculations show again that trajectories of three particles, presented in Fig. 3, replicate the knotted structure, although it is much more challenging from the numerical (and, consequently, experimental) point of view, due to the presence of almost "intersecting" lines.

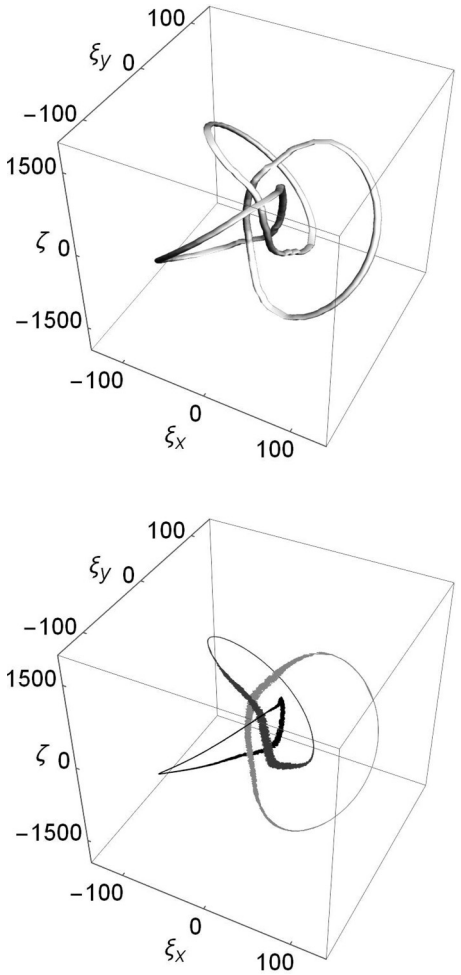

FIG. 3. The nodal line of the light wave representing the (3, 3)-torus knot (upper plot) and the trajectories of three injected particles (lower plot). The values of parameters are the same as before.

The broadening of the trajectories of particles close to the passing points is less visible and depends on the precision of tuning their initial states, which has been successfully implemented in the numerical calculations. Due to the complicated nodal structure, the potential becomes relatively shallow (and with many local minima). Far from the passing points the amplitude of the perpendicular oscillatory motion is strongly suppressed due to the steeper potential valley. The initial conditions satisfied by particles have to be fine tuned so as to appropriately place them in the field and to avoid chaotic motion. This is reflected in the numerical calculations, where trajectories become sensitive to the initial states.

It is difficult to provide a general recipe for the precision of the initial position of the particle so that it runs along the knot line, as this depends on the particular location, especially for more complex structures. For simpler knots, the accuracy of a few wavelengths is sufficient, and, for more sophisticated ones, mostly close to the passing points, it needs to be improved 10 times or even more. This depends to a large extent on the initial cooling of particles. For those with energies measured in neV, the precision can be relaxed; however, this leads to a longer travel time along the nodal line. Generically, most of the kinetic energy is related to very dense oscillations and not to the translational motion of the particle. For instance the whole trajectories of Fig. 3 are realized within the time of order of $10^7\omega^{-1}$. These conditions can be relaxed by using more intense beams, which produces a deeper binding potential.

In the absence of sufficient precision, completely chaotic motion or jumps between nodal lines are probable to occur, examples of which will be presented below. However, even if high accuracy is required to realize a knotted trajectory, it is much easier to achieve it at one (initial) point than to control the motion of the particle with this high accuracy over the entire complex trajectory.

D. The trefoil

A very nontrivial knot known as the trefoil is generated from a polynomial other than the types described with the formula (13). This time it has the form

$$q(u, v) = u^2 - v^3, \tag{37}$$

leading to

$$q_M(\boldsymbol{\xi}, 0) = \left(1 + \xi_x^2 + \xi_y^2\right)\left(1 - \xi_x^2 - \xi_y^2\right)^2 - 8(\xi_x + i\xi_y)^3, \tag{38}$$

and belongs to the larger family of knots obtained from the expression

$$q(u, v) = u^2 - v^n, \tag{39}$$

with $n \in \mathbb{N}$ [53], like the cinqefoil knot ($n = 5$) or the septafoil knot ($n = 7$), etc.

The wave envelope is constructed from $q_M(\boldsymbol{\xi}, 0)$ as in the previous subsections. We define

$$\Psi(\boldsymbol{\xi}, \zeta) = \frac{-i}{2\pi\zeta}\int_0^\infty d\xi' \xi' \int_0^{2\pi} d\phi' e^{\frac{i}{2\zeta}[\xi^2 + \xi'^2 - 2\xi\xi'\cos(\phi - \phi')]} \times e^{-\kappa\xi'^2}[(1 + \gamma^2\xi'^2)(1 - \gamma^2\xi'^2)^2 - 8\gamma^3\xi'^3 e^{3i\phi'}] \tag{40}$$

and integrate first with respect to ϕ',

$$\Psi(\boldsymbol{\xi}, \zeta) = \frac{-i}{\zeta} e^{\frac{i}{2\zeta}\xi^2}\int_0^\infty d\xi' e^{-(\kappa - \frac{i}{2\zeta})\xi'^2}[\xi'(1 + \gamma^2\xi'^2) \times (1 - \gamma^2\xi'^2)^2 J_0(\xi\xi'/\zeta) - 8ie^{3i\phi}\gamma^3\xi'^3 J_3(\xi\xi'/\zeta)], \tag{41}$$

and finally over ξ',

$$\Psi(\boldsymbol{\xi}, \zeta) = e^{-\frac{\kappa\xi^2}{c(\zeta)}}\left(\frac{1}{c(\zeta)} - \frac{2i\gamma^2\zeta}{c(\zeta)^2} - \frac{\gamma^2\xi^2}{c(\zeta)^3} + \frac{8\gamma^4\zeta^2}{c(\zeta)^3} - \frac{8i\gamma^4\xi^2\zeta}{c(\zeta)^4} - \frac{48i\gamma^6\zeta^3}{c(\zeta)^4} - \frac{\gamma^4\xi^4}{c(\zeta)^5} - \frac{72\gamma^6\xi^2\zeta^2}{c(\zeta)^5} + \frac{18i\gamma^6\xi^4\zeta}{c(\zeta)^6} + \frac{\gamma^6\xi^6}{c(\zeta)^7} - \frac{8\gamma^3\xi^3}{c(\zeta)^4}e^{3i\phi}\right). \tag{42}$$

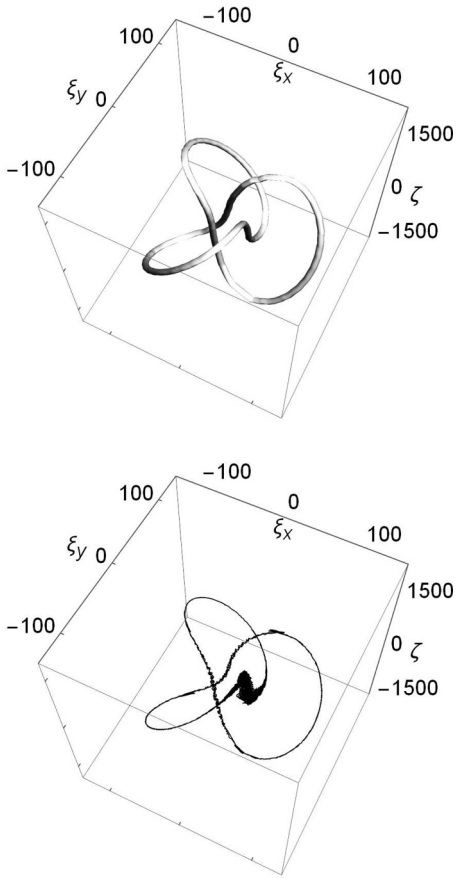

FIG. 4. The nodal line of the light wave representing the trefoil (upper plot) and the trajectory of the injected particle (lower plot). The values of parameters are the same as before.

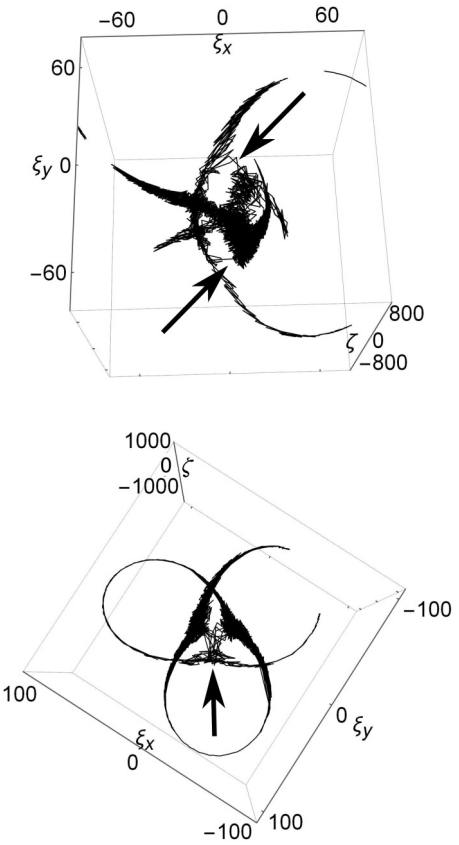

FIG. 5. Jumps between different rings of the (3, 3)-torus knot (upper plot) and different foils of a trefoil (lower plot). Jumping places are marked with arrows.

The corresponding paraxial polynomial may be obtained in the form

$$\begin{aligned} q_p(\boldsymbol{\xi},\zeta) = 1 &- 2i\gamma^2\zeta - \gamma^2\left(\xi_x^2+\xi_y^2\right) + 8\gamma^4\zeta^2 \\ &- 8i\gamma^4\left(\xi_x^2+\xi_y^2\right)\zeta - 48i\gamma^6\zeta^3 - \gamma^4\left(\xi_x^2+\xi_y^2\right)^2 \\ &- 72\gamma^6\left(\xi_x^2+\xi_y^2\right)\zeta^2 + 18i\gamma^6\left(\xi_x^2+\xi_y^2\right)^2\zeta \\ &+ \gamma^6\left(\xi_x^2+\xi_y^2\right)^3 - 8\gamma^3(\xi_x+i\xi_y)^3. \end{aligned} \tag{43}$$

The results of the numerical calculations of the atom trajectory in this case are presented in Fig. 4. It exactly follows the trefoil line, again performing the perpendicular oscillatory motion. The conclusions are similar to those of the (3, 3)-torus knot. Comparable effects can be obtained for the cinquefoil and other knots.

Figure 5 presents the possible jumping of a particle between various nodal lines. The left illustration shows the area of mutual passing of the three rings of the (3,3)-torus knot at some magnification. In this magnification the amplitude of the oscillatory motion appears very high. A particle moving along the first ring, entering the area of the potential valley flattening, increases this amplitude to the extent that there occurs a jump (at the point marked with the arrow) to the second of the rings. After some time, another jump to the third ring takes place. Similarly, the right picture shows the region of multiple jumps between separate trefoil leaves.

In the case of the (3,3)-torus knot, the modification of the initial position in relation to the stable trajectory from Fig. 1 was about 0.5λ, while the initial speed changed by about 50%. However, these values should be treated only as illustrative ones, as they strongly depend on the type of a knot, on the position on it, on the direction of velocity relative to the position vector, and also on the beams' intensities. Lowering the value of β for instance by $2n$ orders of magnitude requires reducing the initial velocity by n orders. The increased imprecision may lead to chaotic motion, although the generic behavior of a particle is rather to maintain a stable trajectory on the nodal line, but not to follow it entirely. This is due to the fact that the depth of the potential valley is varying in different places and the particle can "bounce" and turn back during the translational motion along the nodal line, but still remains on it.

IV. SUMMARY

In conclusion, the paper presents a simple analytical way of obtaining Gaussian light beams with a given knotted topology of the nodal lines starting from the Milnor polynomials with an additional scaling factor. The method is based on the similarity between the paraxial wave equation and the two-dimensional Schrödinger equation. Then it is shown in

a numerical way that neutral, polarizable particles, such as atoms, but also charged particles (electrons) subject to ponderomotive potential, can be forced to follow these knot lines. In all considered cases this result turned out to be feasible upon very precise tuning of the initial positions and velocities of particles. The more braided the nodal structure is, the shallower the created potential is (especially close to the passing points), and more redundant minima appear and more accurate preparation of particles is required.

Various effects are possible in the absence of adequate precision in setting the initial conditions satisfied by a particle: from completely chaotic motion, through jumps between different knot branches, to a stable motion, but only along a section of the knot line.

The results of this work seem applicable, for instance, for precise guiding of particles along prescribed complicated pathways, particularly with the presence of obstacles, for the generation of knotted nanocircuits, or for engineering complex nanoparticles. One potential very important application might be also transferring of the knotted topology of the light beams to the Bose-Einstein condensate and creating stable quantum knots [58–60]. From the theoretical point of view it could be achieved by incorporating the optical potential created by the appropriate superposition of Gaussian beams into the Gross-Pitaevskii equation [61,62]. However, mathematically this seems to be quite a challenge.

ACKNOWLEDGMENT

I would like to thank to Dr. Benjamin Bode for having drawn my attention to the correct nomenclature of knots.

APPENDIX

In this Appendix several integrals needed to find knotted solutions of the paraxial equation are collected:

$$\int_0^{2\pi} d\phi' e^{-i\beta\cos(\phi-\phi')} e^{in\phi'} = 2\pi(-i)^n e^{in\phi} J_n(\beta), \quad \times \text{ for } n = 0, 1, 2, \ldots . \tag{A1}$$

$$\int_0^\infty dx\, x\, e^{-ax^2} J_0(bx) = \frac{1}{2a} e^{-\frac{b^2}{4a}}, \tag{A2}$$

$$\int_0^\infty dx\, x^3\, e^{-ax^2} J_0(bx) = \left(\frac{1}{2a} - \frac{b^2}{8a^3}\right) e^{-\frac{b^2}{4a}}, \tag{A3}$$

$$\int_0^\infty dx\, x^5\, e^{-ax^2} J_0(bx) = \left(\frac{1}{a^3} - \frac{b^2}{2a^4} + \frac{b^4}{32a^5}\right) e^{-\frac{b^2}{4a}}, \tag{A4}$$

$$\int_0^\infty dx\, x^2\, e^{-ax^2} J_1(bx) = \frac{b}{4a^2} e^{-\frac{b^2}{4a}}, \tag{A5}$$

$$\int_0^\infty dx\, x^3\, e^{-ax^2} J_2(bx) = \frac{b^2}{8a^3} e^{-\frac{b^2}{4a}}, \tag{A6}$$

$$\int_0^\infty dx\, x^4\, e^{-ax^2} J_3(bx) = \frac{b^3}{16a^4} e^{-\frac{b^2}{4a}}. \tag{A7}$$

[1] J. Arlt, K. Dholakia, L. Allen, and M. J. Padgett, J. Mod. Opt **45**, 1231 (1997).
[2] F. Flossmann, U. T. Schwarz, and M. Maier, J. Mod. Opt. **52**, 1009 (2005).
[3] S. Sundbeck, I. Gruzberg, and D. G. Grier, Opt. Lett. **30**, 477 (2005).
[4] G. A. Siviloglou, J. Broky, A. Dogariu, and D. N. Christodoulides, Phys. Rev. Lett. **99**, 213901 (2007).
[5] D. L. Andrews, *Structured Light and Its Applications: An Introduction to Phase-Structured Beams and Nanoscale Optical Forces* (Academic, New York, 2008).
[6] S.-H. Lee, Y. Roichman, and D. G. Grier, Opt. Express **18**, 6988 (2010).
[7] P. Zhang, Y. Hu, T. Li, D. Cannan, X. Yin, R. Morandotti, Z. Chen, and X. Zhang, Phys. Rev. Lett **109**, 193901 (2012).
[8] M. Babiker, D. L. Andrews, and V. E. Lembessis, J. Opt. **21**, 013001 (2019).
[9] L. Allen, M. W. Beijersbergen, R. J. C. Spreeuw, and J. P. Woerdman, Phys. Rev. A **45**, 8185 (1992).
[10] M. Padgett, J. Arlt, N. Simpson, and L. Allen, Am. J. Phys. **64**, 77 (1996).
[11] J. Arlt, T. Hitomi, and K. Dholakia, Appl. Phys. B **71**, 549 (2000).
[12] J. Durnin, J. Opt. Soc. Am. A **4**, 651 (1987).
[13] J. Durnin, J. J. Miceli, and J. Eberly, Phys. Rev. Lett. **58**, 1499 (1987).
[14] K. Volke-Sepulveda, V. Garcés-Chévez, S. Chávez-Cerda, J. Arlt, and K. Dholakia, J. Opt. B **4**, S82 (2002).
[15] I. Białynicki-Birula, Z. Białynicka-Birula, and N. Drozd, in *The Angular Momentum of Light*, edited by D. L. Andrews and M. Babiker (Cambridge University Press, Cambridge, 2012).
[16] T. Radożycki, Phys. Rev. A **100**, 063412 (2019).
[17] M. Chen, S. Huang, X. Liu, Y. Chen, and W. Shao, Appl. Phys. B **125**, 184 (2019).
[18] N. K. Efremidis, Z. Chen, M. Segev, and D. N. Christodoulides, Optica **6**, 686 (2019).
[19] J. C. Gutierrez-Vega, R. M. Rodriguez-Dagnino, M. D. I. Castillo, and S. Chavez-Cerda, in Optical Pulse and Beam Propagation III, San Jose, 2001, edited by Y. B. Band [Proc. SPIE 4271, 73 (2001)].
[20] S. Yan, M. Li, B. Yao, X. Yu, M. Lei, D. Dan, Y. Yang, J. Min, and T. Peng, Phys. Lett. A **379**, 983 (2015).
[21] W. Thomson, Philos. Mag. **34**, 15 (1867).
[22] P. A. M. Dirac, Proc. R. Soc. London A **133**, 60 (1931).
[23] Y. Aharonov and D. Bohm, Phys. Rev. **115**, 485 (1959).
[24] A. F. Rañada, Lett. Math. Phys. **18**, 97 (1989).
[25] W. T. M. Irvine and D. Bouwmeester, Nat. Phys. **4**, 716 (2008).
[26] I. M. Besieris and A. M. Shaarawi, Opt. Lett. **34**, 3887 (2009).
[27] H. Kedia, I. Białynicki-Birula, D. Peralta-Salas, and W. T. M. Irvine, Phys. Rev. Lett. **111**, 150404 (2013).
[28] M. Arrayás and J. L. Trueba, J. Phys. A **48**, 025203 (2015).
[29] M. Arrayás, D. Bouwmeester, and J. L. Trueba, Phys. Rep. **667**, 1 (2017).
[30] M. V. Berry and M. R. Dennis, Proc. R. Soc. London A **457**, 2251 (2001).
[31] M. R. Dennis, New J. Phys. **5**, 134 (2003).

[32] M. R. Dennis, R. P. King, B. Jack, K. O'Holleran, and M. J. Padgett, Nat. Phys. **6**, 118 (2010).
[33] D. Kleckner and W. T. M. Irvine, Nat. Phys. **9**, 253 (2013).
[34] A. J. J. M. de Klerk, R. I. van der Veen, J. W. Dalhuisen, and D. Bouwmeester, Phys. Rev A **95**, 053820 (2017).
[35] D. Sugic and M. R. Dennis, J. Opt. Soc. Am. A **35**, 1987 (2018).
[36] J. Leach, M. R. Dennis, J. Courtial, and M. J. Padgett, Nature (London) **432**, 165 (2004).
[37] J. Leach, M. R. Dennis, J. Courtial, and M. J. Padgett, New J. Phys. **7**, 55 (2005).
[38] E. R. Shanblatt and D. G. Grier, Opt. Express **19**, 5833 (2011).
[39] S. J. Tempone-Wiltshire, S. P. Johnstone, and K. Helmerson, Sci. Rep. **6**, 24463 (2016).
[40] N. B. Delone and V. P. Krainov, Phys. Usp. **42**, 669 (1999).
[41] S. Chu, J. E. Bjorkholm, A. Ashkin, and A. Cable, Phys. Rev. Lett. **57**, 314 (1986).
[42] J. D. Miller, R. A. Cline, and D. J. Heinzen, Phys. Rev. A **47**, R4567 (1993).
[43] R. Grimm, M. Weidemüller, and Y. B. Ovchinnikov, Adv. At. Mol. Opt. Phys. **42**, 95 (2000).
[44] D. J. Stevenson, F. J. Gunn-Moore, and K. Dholakia, J. Biomed. Opt. **15**, 041503 (2010).
[45] F. M. Fazal and S. M. Block, Nat. Photon. **5**, 318 (2011).
[46] *Optical Tweezers: Methods and Applications*, edited by M. Padgett, J. Molloy, and D. McGloin, Series in Optics and Optoelectronics (CRC, Boca Raton, FL, 2010).
[47] M. Woerdemann, *Structured Light Fields: Applications in Optical Trapping, Manipulation, and Organisation* (Springer, Berlin, 2012).
[48] R. W. Bowman and M. J. Padgett, Rep. Prog. Phys. **76**, 026401 (2013).
[49] D. G. Grier, Nature (London) **424**, 810 (2003).
[50] D. S. Bradshaw and D. L. Andrews, Eur. J. Phys. **38**, 034008 (2017).
[51] M. Arrayás and J. L. Trueba, J. Phys. A **43**, 235401 (2010).
[52] K. Brauner, Abh. Math. Semin. Univ. Hamburg **6**, 1 (1928).
[53] R. P. King, Knotting of Optical Vortices, Ph.D. Thesis, University of Southampton, 2010 (unpublished).
[54] B. Bode, M. R. Dennis, D. Foster, and R. P. King, Proc. R. Soc. A **473**, 20160829 (2017).
[55] J. W. Milnor, *Singular Points of Complex Hypersurfaces*, Annals of Mathematics Studies (Princeton University Press, Princeton, 1968).
[56] E. Karimi, G. Zito, B. Piccirillo, L. Marrucci, and E. Santamato, Opt. Lett. **32**, 3053 (2007).
[57] A. E. Siegman, *Lasers* (University Science Books, Mill Valley, CA, 1986).
[58] D. Proment, M. Onorato, and C. F. Barenghi, Phys. Rev. E **85**, 036306 (2012).
[59] D. Proment, M. Onorato, and C. F. Barenghi, J. Phys.: Conf. Ser. **544**, 012022 (2014).
[60] C. W. Duncan, C. Ross, N. Westerberg, M. Valiente, B. J. Schroers, and P. Öhberg, Phys. Rev. A **99**, 063613 (2019).
[61] E. P. Gross, Nuovo Cimento **20**, 454 (1961).
[62] L. P. Pitaevskii, Sov. Phys. JETP. **13**, 451 (1961).